EBioMedicine 67 (2021) 103372

Contents lists available at ScienceDirect

EBioMedicine

journal homepage: www.elsevier.com/locate/ebiom

Research paper

Near-infrared photoimmunotherapy targeting GPR87: Development of a humanised anti-GPR87 mAb and therapeutic efficacy on a lung cancer mouse model

Hirotoshi Yasui[a], Yuko Nishinaga[a], Shunichi Taki[a], Kazuomi Takahashi[a], Yoshitaka Isobe[a], Misae Shimizu[b], Chiaki Koike[b], Tetsuro Taki[c], Aya Sakamoto[d], Keiko Katsumi[d], Keisuke Ishii[d], Kazuhide Sato[a,b,e,f,*]

[a] Respiratory Medicine, Nagoya University Graduate School of Medicine, 65, Tsurumai-cho, Showa-ku, Nagoya 466-8560, Aichi, Japan
[b] Nagoya University Institute for Advanced Research, Advanced Analytical and Diagnostic Imaging Center (AADIC) / Medical Engineering Unit (MEU), B3 Unit, 65, Tsurumai-cho, Showa-ku, Nagoya 466-8560, Aichi, Japan
[c] Department of Pathology, Nagoya University Graduate School of Medicine, 65, Tsurumai-cho, Showa-ku, Nagoya 466-8560, Aichi, Japan
[d] Perseus Proteomics, Inc., 4-7-6, Komaba 153-0041, Meguro-ku, Tokyo, Japan
[e] FOREST- Souhatsu, CREST, JST
[f] Nagoya University Institute for Advanced Research, S-YLC, Furo-cho, Chikusa-ku, Nagoya 464-8601, Aichi,, Japan

ARTICLE INFO

Article History:
Received 13 February 2021
Revised 25 March 2021
Accepted 16 April 2021
Available online xxx

Keywords:
Near infrared photoimmunotherapy
IRDye700
Malignant pleural mesothelioma
Lung cancer
GPR87
G-protein receptor

ABSTRACT

Background: GPR87 is a G-protein receptor that is specifically expressed in tumour cells, such as lung cancer, and rarely expressed in normal cells. GPR87 is a promising target for cancer therapy, but its ligand is controversial. Near-infrared photoimmunotherapy (NIR-PIT) is a novel cancer therapy in which a photosensitiser, IRDye700DX (IR700), binds to antibodies and specifically destroys target cells by irradiating them with near-infrared-light. Here, we aimed to develop a NIR-PIT targeting GPR87.
Methods: We evaluated the expression of GPR87 in resected specimens of lung cancer and malignant pleural mesothelioma (MPM) resected at Nagoya University Hospital using immunostaining. Humanised anti-GPR87 antibody (huGPR87) was generated by introducing CDRs from mouse anti-GPR87 antibody generated by standard hybridoma method. HuGPR87 was conjugated with IR700 and the therapeutic effect of NIR-PIT was evaluated *in vitro* and *in vivo* using lung cancer or MPM cell lines.
Findings: Among the surgical specimens, 54% of lung cancer and 100% of MPM showed high expression of GPR87. It showed therapeutic effects on lung cancer and MPM cell lines *in vitro*, and showed therapeutic effects in multiple models *in vivo*.
Interpretation: These results suggest that NIR-PIT targeting GPR87 is a promising therapeutic approach for the treatment of thoracic cancer.
Funding: This research was supported by the Program for Developing Next-generation Researchers (Japan Science and Technology Agency), KAKEN (18K15923, 21K07217, JSPS), FOREST-Souhatsu, CREST (JST).

1. Introduction

The most common cause of cancer death in the world is lung cancer [1,2]. Malignant pleural mesothelioma (MPM) derives from mesothelial cells such as the pleura and peritoneum, mainly after exposure to asbestos. Although the use of asbestos is regulated, the number of mesothelioma cases is increasing [3]. There is no cure, and treatment options include radiation therapy, targeted therapy, chemotherapy, or multidisciplinary treatment. Surgery is considered in some early-stage patients [4]. Both lung cancer and malignant mesothelioma are diseases with poor prognoses, and there is a need for new treatments.

GPR87 is a common G-protein receptor that is specifically expressed on various tumour cells such as lung, pancreatic, bladder, skin, and cervical cancers, and has been reported to be associated with tumour cell growth [5–10]. High GPR87 expression in lung and pancreatic cancer is associated with a worse prognosis [11,12]. Therefore, GPR87 is attracting attention as a promising cancer therapeutic target [8–10,13,14]. However, the development of antitumour agents targeting GPR87 has not progressed, and there are only a few preclinical reports of gene therapy [12,15].

* Corresponding author.
E-mail address: k-sato@med.nagoya-u.ac.jp (K. Sato).

https://doi.org/10.1016/j.ebiom.2021.103372

Research in context

Evidence before this study

Thoracic malignancies, such as lung cancer and malignant pleural mesothelioma (MPM) still remain poor prognosis, and require the development of new therapies.

GPR87 is a G-protein receptor that is found to be expressed in various cancers, but is poorly expressed in normal cells. GPR87 is a promising malignancy target, however, there have only been a few preclinical reports of gene therapy. Therefore, the development of therapeutic agents for GPR87 is desirable.

Near-infrared photoimmunotherapy (NIR-PIT) is a new method of cancer treatment with antibody-dye conjugates, which are composed of antibodies and IR700Dye, a photosensitive substance, coupled with NIR-light. By irradiating the antibody-dye conjugate with NIR-light, the dye rapidly changes from hydrophilic to hydrophobic, and the process damages the cell membrane, causing cell death. Currently, NIR-PIT targeting EGFR is in clinical use for head and neck cancer.

Added value of this study

High expression of GPR87 was confirmed in clinical resection specimens of lung cancer (adenocarcinoma, squamous cell carcinoma, and small cell carcinoma) and MPM at our institution. High expression of GPR87 was also confirmed in cell lines of lung cancer and MPM.

To perform GPR87-targeting NIR-PIT, we generated humanised GPR87 antibodies and created antibody-dye conjugate. *In vitro* NIR-PIT targeting GPR87 only injured GPR87-expressing cells and did not affect non-targeted cells. *In vivo*, it significantly suppressed tumour growth in several mouse models.

Implications of all the available evidence

This study provides evidence that GPR87 is frequently highly upregulated in lung cancer and MPM and preclinical evidence that NIR-PIT targeting GPR87 is a promising treatment for lung cancer and MPM.

Near-infrared photoimmunotherapy (NIR-PIT) is an emerging cancer modality, where IRDye700DX (IR700), a photosensitiser, is bound to an antibody, and near-infrared-light irradiation specifically destroys the targeting cell [16,17]. A Phase 2a study of cetuximab-IR700 (Cetuximab Sarotalocan Sodium) in patients with locally recurrent or advanced head and neck squamous cell cancer (HNSCC) showed a 43% overall response rate and an 86.7% disease control rate [18]. An international phase III clinical trial is underway for patients with HNSCC (LUZERA-301, NCT03769506). In September 2020, the Japanese Agency approved NIR-PIT for recurrent HNSCC.

Monoclonal antibodies (mAbs) are used in NIR-PIT, and almost all mAbs currently being used clinically are humanised or human antibodies. The use of mouse antibodies is limited because up to 50% of patients have a human anti-mouse antibody (HAMA) response [19]. The HAMA response is significantly reduced or abolished by chimerisation and humanisation.

Here, we created a humanised antibody from a mouse anti-GPR87 antibody (moGPR87ab) to avoid the HAMA response. Moreover, we developed a NIR-PIT targeting GPR87 using a newly developed humanised anti-GPR87 antibody (huGPR87ab).

2. Methods

2.1. Study design and ethics

The aim of this study was to develop NIR-PIT targeting GPR87, and the therapeutic targets were MPM and lung cancer. All *in vivo* procedures were performed in accordance with the Nagoya University Animal Care and Use Committee's "Guide for the Management and Use of Laboratory Animal Resources" (approval numbers 2017−29,438, #2018−30,096, # 2019−31,234, #2020−20,104). The use of specimens from patients was approved by the Ethics Committee of the Nagoya University Clinical Research Committee (Approval No. 2018−0046).

2.2. Immunostaining of surgically resected lung cancer and malignant pleural mesothelioma specimens

We performed GPR87 immunostaining to resected specimens from patients pathologically diagnosed with lung cancer or malignant pleural mesothelioma (MPM) who underwent surgery at Nagoya University Hospital (from April 2004 until December 2015). The staining of the cytoplasm or the cell membrane, assessed by two or more physicians, was defined as GPR87 positive, regardless the intensity.

After formalin fixation, paraffin-embedded surgical specimens were thinly sliced to a thickness of 4 μm and placed on a glass slide. Epitope retrieval was performed employing a pH 6 buffer (Epitope Retrieval Solution pH 6; Leica Biosystems, Nussloch, Germany; cat # RE7113-CE) and an autoclave. The sections were treated for 15 min at 15−25 °C with protein blocking agent (Protein Block, Serum-Free, Liquid form; Agilent, Santa Clara, CA, USA; cat # X090930−2) to block nonspecific staining. We used rabbit polyclonal anti-GPR-87 antibody (Novus Biologicals, LLC, Centennial, Colorado, USA; cat # NLS1584). The samples were treated with 0.3% H_2O_2 (in absolute methanol) for 15 min, and horseradish peroxidase-polymer secondary antibody (EnVision+ system HRP-labeled polymer anti-rabbit; Agilent, Santa Clara, CA, USA; cat Dako #K4003) to stop endogenous peroxidase activity. Colorimetric development was performed with 3,3-diaminobenzidine (ImmPACT DAB Substrate; Vector, Burlingame, CA, USA; cat # SK-4105) and hematoxylin. GPR87 expression was tested at 100 × and 400 × magnification under a brightfield microscope.

Mouse subcutaneous PC9 tumours were used as a positive control, in which GPR87 was highly expressed. After the mouse were euthanised, it was perfusion-fixed in 4% paraformaldehyde, and the tumours were harvested and paraffin-embedded. In the specimen of PC9 tumours, both the plasma membrane and the cytoplasm in the PC9 tumour cells were stained (Fig. S1). Therefore, positive staining was defined as the staining of > 10% of the tumour cell at any intensity. IHC status was evaluated by at least two respiratory physicians (H.Y, Y.N, S.T, K.T, Y.I, K.S) and one pathologist (T.T).

2.3. Reagents

Water-soluble, silicon-phthalocyanine derivative IRDye 700DX NHS ester was purchased from LI-COR Biosciences (Lincoln, Nebraska USA) (cat # 929−70,010).

2.4. Humanisation of mouse antibody

MoGPR87ab was generated using the standard hybridoma methodology. The heavy and light chain variable regions (VH and VL) from the hybridoma cell line were recovered by RT-PCR using specific primers for mouse antibody variable genes. We then constructed a humanised antibody by grafting the complementarity-determining regions (CDRs) onto the most similar human germline sequences (Fig. 1).

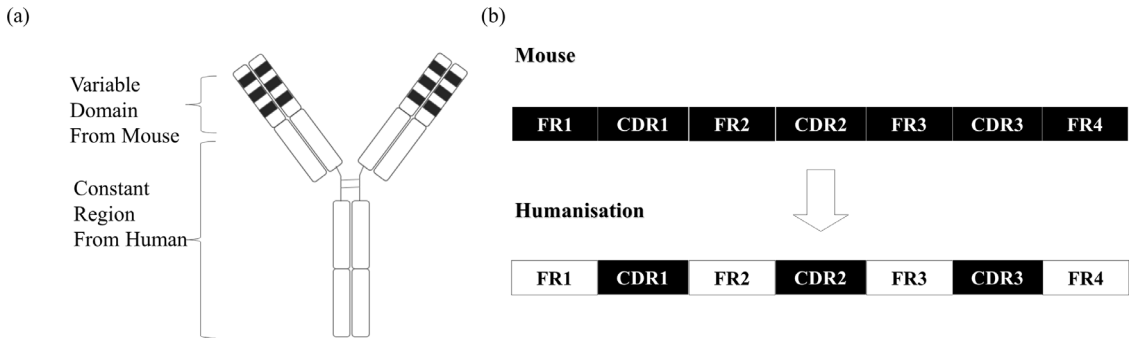

Fig. 1. Structure of the humanised antibody and variable domain.
(**a**) Structure of the humanised antibody. (**b**) Structure of the variable domains (VH or VL). CDR1, 2, and 3 are the complementarity-determining regions. FR1, 2, 3, and 4 are the framework regions. Mouse sequence is in black, and human sequence is in white.

2.5. Expression and purification

The humanised VH and VL genes were synthesized and codon optimized for mammalian cell expression. The expression plasmid of the heavy chain (H plasmid) was constructed by cloning the VH sequence into the expression vector pCXN2 in frame with the human IgG_1 Fc region. The expression plasmid of the light chain (L plasmid) was constructed by cloning the VL and constant region sequence into the expression vector pCXN2. Both the H plasmid and L plasmid were transfected into the HEK293 cell line. The resulting humanised GPR87 antibody was further purified by Ab-Capcher ExTra (Protenova, Kagawa, Japan; cat # P-003–2), and the purified product was designated as huGPR87ab.

2.6. Cell lines

3T3 (mouse fibroblast; RRID) (CVCL_0594), PC9 (human non-small-cell lung adenocarcinoma [NSLAC]) (RRID: CVCL_B260), H1975 (human NSLAC) (RRID: CVCL_1511), H661 (human lung large cell carcinoma) (RRID: CVCL_1577), H226 (human non-small-cell lung squamous cell carcinoma [NSLSCC]) (RRID: CVCL_1544), MSTO-211H (human MPM) (RRID: CVCL_1430), and H2373 (human MPM) (RRID: CVCL_A533) cells were obtained from the American Type Culture Collection (ATCC); SBC3 (RRID: CVCL_1678) and SBC5 (RRID: CVCL_1679) cell lines, which are both derived from Japanese patients with small-cell lung cancer (SCLC), were obtained from the Japanese Collection of Research Bioresources (JRBC)(Osaka, Japan). The *cdk4/hTERT*-immortalised normal human bronchial epithelial cell line HBEC3-KT (RRID: CVCL_X491) was obtained from the Hamon Center collection (University of Texas Southwestern Medical Center, Dallas, TX, USA) [20]. GPR87-CHO cells, forcibly expressing GPR87 in Chinese hamster ovarian cells, were provided by Perseus Proteomics.

Luciferase-expressing PC9, SBC5, and H2373 cell lines were made by transfecting RediFect Red-FLuc lentiviral particles (PerkinElmer, Waltham, MA, USA; cat # CLS960002), as previously reported [21,22]. High, stable expression of luciferase was validated after performing over 20 passages.

2.7. Cell culture

Cells were cultured in RPMI 1640 medium (Thermo Fisher Scientific, Rockford, IL, USA; cat # 11,875,093) supplemented with 10% foetal bovine serum, penicillin (100 IU/mL), and streptomycin (100 mg/mL) (Thermo Fisher Scientific; cat # 15,140,148).

2.8. Synthesis of IR700-conjugated anti-GPR87 antibody

Anti-GPR87 antibody (GPR87ab) (1 mg; 6.8 nmol) was incubated with IR700 NHS ester (LI-COR Biosciences, Lincoln, NE, USA) (66.8 mg; 34.2 nmol, 5 mmol/L in DMSO) in 0.1 mol/L Na_2HPO_4 (pH 8.6) at 15–25 °C for 1 h. The mixture was purified employing a Sephadex G50 column (PD-10, GE Healthcare; Piscataway, NJ, USA; cat # 17,085,101). The protein concentration was decided employing a Coomassie Plus protein assay kit (Thermo Fisher Scientific; cat # 23,236) by spectroscopically (at 595 nm) (Novaspec Plus; GE Healthcare; cat # 10,187,054). The concentration of IR700 was spectroscopically measured at 689 nm to verify the amount of Ab-conjugated fluorophores [23–25]. The synthesis was controlled in order that a mean of three IR700 molecules were sure to a single antibody; these GPR87ab conjugates with IR700 were abbreviated to as GPR87ab-IR700.

2.9. SDS-PAGE

We examined the quality for the conjugate with SDS-PAGE as previously [26–29]; diluted naked GPR87ab was used as a non-conjugated control. The fluorescent bands were measured with fluorescence imagers; an Odyssey Imager (LI-COR Biosciences; cat # 9141–00) or Pearl Imager (LI-COR Biosciences; cat # 9430–00) using a 700-nm fluorescence channel [24].

2.10. Flow cytometry

Flow cytometry analysis was performed as previously reported [30,31]. Cells (1×10^5) were seeded onto 12-well plates and incubated with moGPR87ab-IR700 or huGPR87ab-IR700 at 10 μg/mL for 12 h at 37 °C. The medium was replaced with PBS after washing twice. To avoid the effect of trypsin on the binding of antibody to cells, cells were stripped from the plate by pipetting, and IR700 fluorescence was evaluated in 10,000 cells with a flow cytometer (Gallios, Beckman Coulter; cat # B43618). To test specific binding to GPR87, a blocking study was performed with PC9-cells that were incubated with excess huGPR87ab beforehand. To stop binding of the huGPR87ab to the Fab region, huGPR87ab-IR700 binding was evaluated after incubating 3T3 and HBEC3 cells with the CD16 antibody (10 μg/mL; CD16/CD32 mAb [clone 93], Thermo Fisher Scientific; RRID: AB_467,133) for 12 h.

2.11. Fluorescence microscopy

To detect the antigen-specific localisation of IR700 conjugates, fluorescence microscopy was done (A1Rsi, Nikon Instech, Tokyo, Japan). Cells (2×10^4) were seeded onto cover glass-bottomed dishes and incubated for 8 h. huGPR87ab-IR700 was then added to the culture medium at 10 μg/mL for single culture and 1 μg/mL for co-culture and incubated at 37 °C for 12 h. The cells were then washed twice with PBS. Propidium iodide (PI, Final 2 μg/mL; Thermo Fischer Scientific; cat # P1304MP) or Sytox Blue (1:500; Thermo Fischer Scientific; cat # S34857) was added to the media at 30 min before observation to stain the necrotic dead cells. The cells were then exposed to NIR-light (64 J/cm^2), and microscopic images were obtained [30–33].

2.12. In vitro *NIR-PIT*

Cells (1×10^5) were spread into a 12-well plate, 10 μg/mL of huGPR87-IR700 was added to the medium on the next day, and incubate for 12 h at 37 °C. Then, the medium was replaced with PBS after washing twice. The cells were irradiated with an NIR (670−710 nm wavelength) light-emitting diode (L690−66−60; Ushio-Epitex, Kyoto, Japan). The particular power density (mW/cm^2) was measured with an optical electric-power metre (PM100; Thorlabs, Newton, NJ, USA), as previously [34].

2.13. *Cytotoxicity/phototoxicity assay*

Luciferase activity was used to quantitatively measure the *in vitro* cytotoxic effects of NIR-PIT with huGPR87ab-IR700. For luciferase activity, 200 μL of 150 μg/mL of D-luciferin-containing media (GoldBio, St Louis, MO, USA) was added to PBS-washed cells 24 h after NIR-PIT. The cells were then analysed on a bioluminescence plate reader (Powerscan4; BioTek, Winooski, VT, USA; cat # BT-S4LFPTAD) at 24 h after NIR-PIT, as previously reported [30,35]

2.14. *Animal and tumour models*

All *in vivo* procedures were conducted in compliance with the local Animal Care and Use Committee of Nagoya University. Female 8-to-12-week-old homozygote athymic nude mice (weighing 18−22 g) were purchased from Chubu Kagaku Shizai (Chikusa, Nagoya, Japan; cat # BALB/cSlc-nu/nu). All mice were housed at 20−25 °C in a 12-hour light/dark cycle, and were anesthetised with isoflurane before conducting any procedures. Every effort was made to reduce the number of animals used, with a total of 26 mice. All mice analysed have been basically included in the results. As this was a proof-of-concept study, the sample size for each animal study was determined based on previous experience and we usually used a minimum of five mice in each experimental group. When comparative intervention experiments were carried out, they were randomly assigned. Mice belonging to different treatment groups were housed in different cages to avoid confounding factors. All study arms were open-label.

Two million PC9-luc cells were injected subcutaneously into one side of the dorsum. Tumour volume was measured 9 days after subcutaneous implantation of tumour cells; mice with small tumours and whose diameter could not be measured were excluded. To work out tumour volume, the maximum length of major axis (length) and length of minor axis (width) were measured with an external caliper. Tumour volumes supported on caliper measurements were calculated using the subsequent formula: tumour volume = length $\times$ width^2 $\times$ 0.5. The mice were euthanised using CO_2 asphyxiation when tumours exceeded 15 mm long. To make a pleural dissemination model, two million PC9-luc cells were injected into the pleural cavity from the right intercostal space with a 30-G needle [36]. After injection, the mice were rolled in order that the cells spread throughout the pleura [30,37].

2.15. In vivo *bioluminescence imaging (BLI)*

D-luciferin (15 mg/mL, 200 μL) was injected to mice intraperitoneally 9 days after subcutaneous cell transplantation or 5 days after thoracic cavity cell transplantation, and luciferase activity was measured using an IVIS imaging system (IVIS Spectrum CT; Perkin Elmer). Mice with no measurable luciferase activity were excluded (failure to make xenograft). Regions of interest were identified on the tumours for the subcutaneous transplantation model and on the ventral chest for the pleural disseminated model, and luciferase luminescence was quantified.

2.16. In vivo *fluorescence imaging*

IR700 fluorescence images were captured before therapy with a fluorescence imager (Pearl Trilogy, LI-COR Biosciences)[38,39].

2.17. In vivo *biodistribution imaging*

Mice with subcutaneous tumours at 9 days after cell transplantation, fed white food for 1 week, are injected intravenously with 200 μg of huGPR87-IR700. 700 nm fluorescence images and white images are acquired with Pearl Trilogy (LI-COR) immediately before injection and at 30 min, 1, 2, 3, 6, 12, 24, 48 and 72 h after injection. The 700 nm fluorescence intensity of the tumour, liver, normal skin and background will be measured. Fluorescence intensity was calculated on a (target - background), and the target to normal skin ratio was calculated as (target - background) / (normal skin - background).

In order to assess the specificity of the antibodies *in vivo*, blocking studies were performed. Three hundred μg of GPR87hu or control IgG antibody was injected via tail vein; then GPR87hu-IR700 (50 μg) was injected 24 h after the injection. The 700 nm fluorescence images were taken immediately before, and 30 min, 1, 2, 3, 6, 9 and 24 h after injection of GPR87hu-IR700.

2.18. In vivo *local GPR87-targeted NIR-PIT*

Mice with a single-dorsum xenograft were randomised into two groups as follows: no treatment (neither GPR87hu-IR700 injections nor NIR-light exposure) (control) and huGPR87ab-IR700 injection followed by NIR-light irradiation (PIT). The mice were injected with 200 μg of huGPR87-IR700 on day −1 (9 days after tumour cell injection into mice) and irradiated with NIR-light laser at 50 J/cm^2 on day 0 and again at 100 J/cm^2 on day 1 at 100 mW/cm^2. Tumour volume and luciferase activity were measured immediately before administration of huGPR87-IR700 (day-1), and on day 0 and 1 before NIR-irradiation, and on day 2, 3, 4 and 7. Tumour volume was the primary endpoint for measuring treatment effect [30,40,41]. Mice seeded with pleura were injected with 200 μg of huGPR87ab-IR700 on day 0 (5 days after tumour cell injection into the mice), and therefore the larger tumour was irradiated with NIR-light laser at 45 J/cm^2 at 60 mW/cm^2 on day 1. Luciferase activity was measured immediately before administration of huGPR87-IR700 (day 0) and on day 1 (before NIR-irradiation), 2, 3 and 4. The primary endpoint for measuring therapeutic efficacy was luciferase activity. The location of the tumour was confirmed via BLI prior to NIR-irradiation in both the subcutaneous and pleural disseminated model; the NIR-laser was directed only at the tumour and the rest of the body was shielded by aluminium foil [30,36].

2.19. *Statistics*

The experimental data are displayed as the means ± SEM.

Statistical analyses were done with the Prism version 7 software (GraphPad, San Diego, CA, USA). For 2-group comparisons, the unpaired two-sided Student's *t*-test was used. The statistically differences were considered significant if *p*-values <0.05 ($^*p < 0.05$, $^{**}p < 0.001$). All data were collected in Microsoft Excel and GraphPad Prism 7.

2.20. *Role of funding sources*

Funders only provided funding, and had no role in the study design, data collection, data analysis, interpretation, and writing of the report.

3. Results

3.1. Immunostaining of human resected lung cancer and MPM surgical specimens

Thirty NSLAC, 29 NSLSCC, 8 SCLC, and 9 MPM samples were collected and stained according to the protocol. Fifteen (50%) NSLAC, 19 (65.5%) NSLSCC, 4 (37.5%) SCLC, and all (100%) MPM samples were GPR87 positive (Fig. 2a and b). The GPR87 positivity rates for NSLAC and NSLSCC were consistent with those reported in previous studies [5,8]. These data supported the rationale and motivation to develop GPR87-targeted therapy.

3.2. Conjugation of the GPR87ab with IR700DX

The integrity of the huGPR87ab-IR700 conjugate was confirmed by observing strong IR700-fluorescence, which was detected in the band of huGPR87ab, while huGPR87ab alone had no detectable fluorescent signals on SDS-PAGE (Fig. 3a). Similarly, we confirmed the conjugation of moGPR87ab-IR700 (data not shown).

On binding with GPR87-CHO cells, which were stably GPR87-overexpressing strains, both moGPR87ab-IR700 and huGPR87ab-IR700 showed similar reactions; almost no signals were observed in either 3T3 mouse fibroblasts or human normal bronchial epithelial cell line HBEC3. However, huGPR87ab-IR700 showed higher IR700 fluorescence than moGPR87ab-IR700 in the human lung cancer cell line PC-9 (Fig. 3b). During flow cytometric assays, PC9 with huGPR87ab-IR700 signals was blocked following the addition of excess huGPR87ab (Fig. 3c), confirming that huGPR87ab-IR700 bound to GPR87 proteins.

These results indicated that huGPR87ab and IR700 were conjugated properly, and the binding was stronger with huGPR87ab than with moGPR87ab-IR700.

3.3. In vitro characterisation of the specific binding of huGPR87-IR700 to GPR87

The fluorescent signals obtained with huGPR87ab-IR700 from H1975 (NSLAC), H661 (large cell lung carcinoma), H226 (NSLSCC), SBC3, SBC5 (SCLC), MSTO-211H, and H2373 (MPM) were evaluated using flow cytometry. Fluorescent signals from lung carcinoma and malignant mesothelioma cells were higher for huGPR87ab-IR700 than for moGPR87ab-IR700 (Fig. 3d). These data indicated that GPR87 is widely expressed, and huGPR87ab-IR700 had sufficient binding affinity to lung carcinoma and malignant mesothelioma cell

(a)

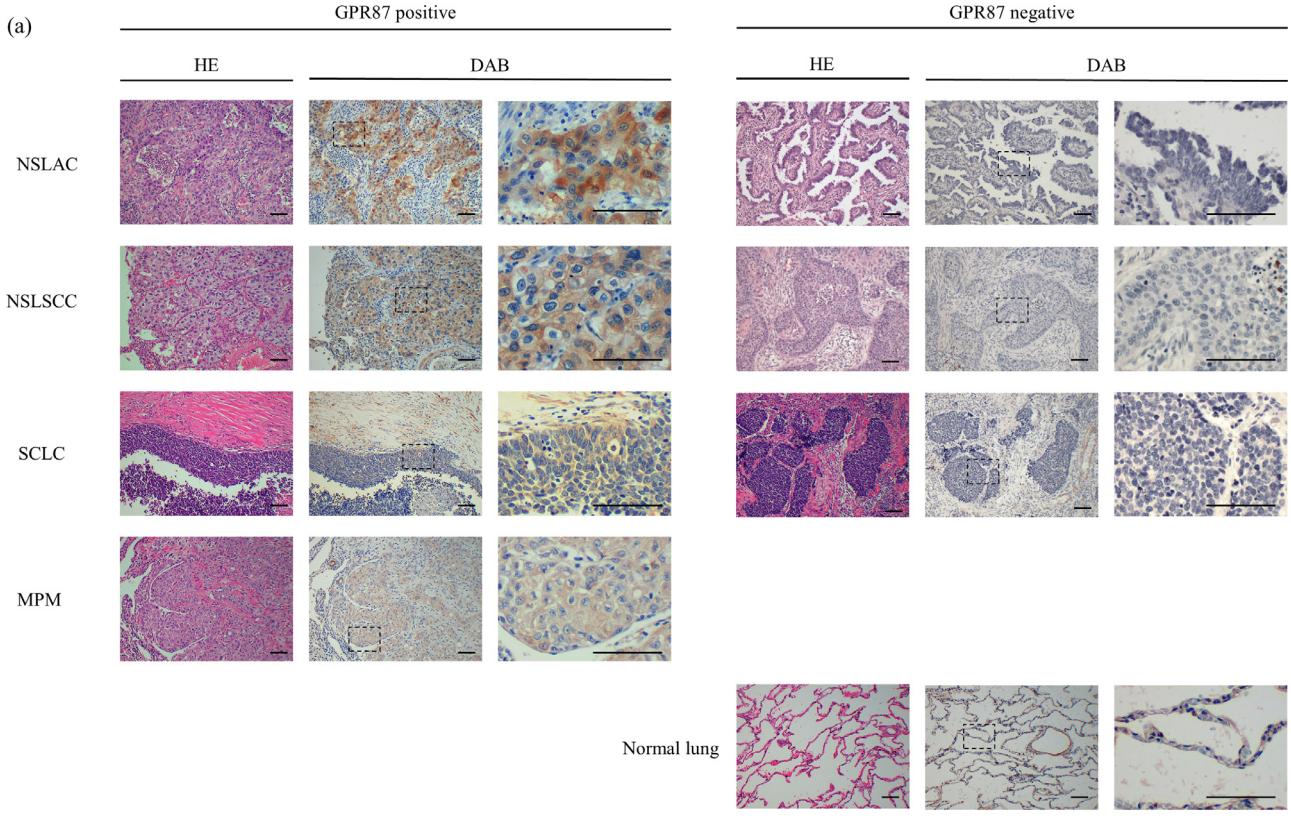

(b)

NSLAC	NSLSCC	SCLC	MPM
15/30 (50%)	19/29 (65.5%)	3/8 (37.5)	8/8 (100%)

Fig. 2. Immunohistochemical staining of resected surgical specimens.
(**a**) Hematoxylin-eosin and GPR87 staining in GPR87-positive and GPR87-negative non-small-cell lung adenocarcinoma (NSLAC), non-small-cell lung squamous cell carcinoma (NSLSCC), small-cell lung cancer (SCLC), and malignant pleural mesothelioma (MPM). Scale bars, 100 μm. Immunostaining for the GPR87 positive PC-9 tumours was obtained as a positive control (Fig. S1). (**b**) The number and proportion of GPR87 positive samples in our institute is shown. Samples in which >10% of the cells show staining at any intensity are considered GPR87 positive.

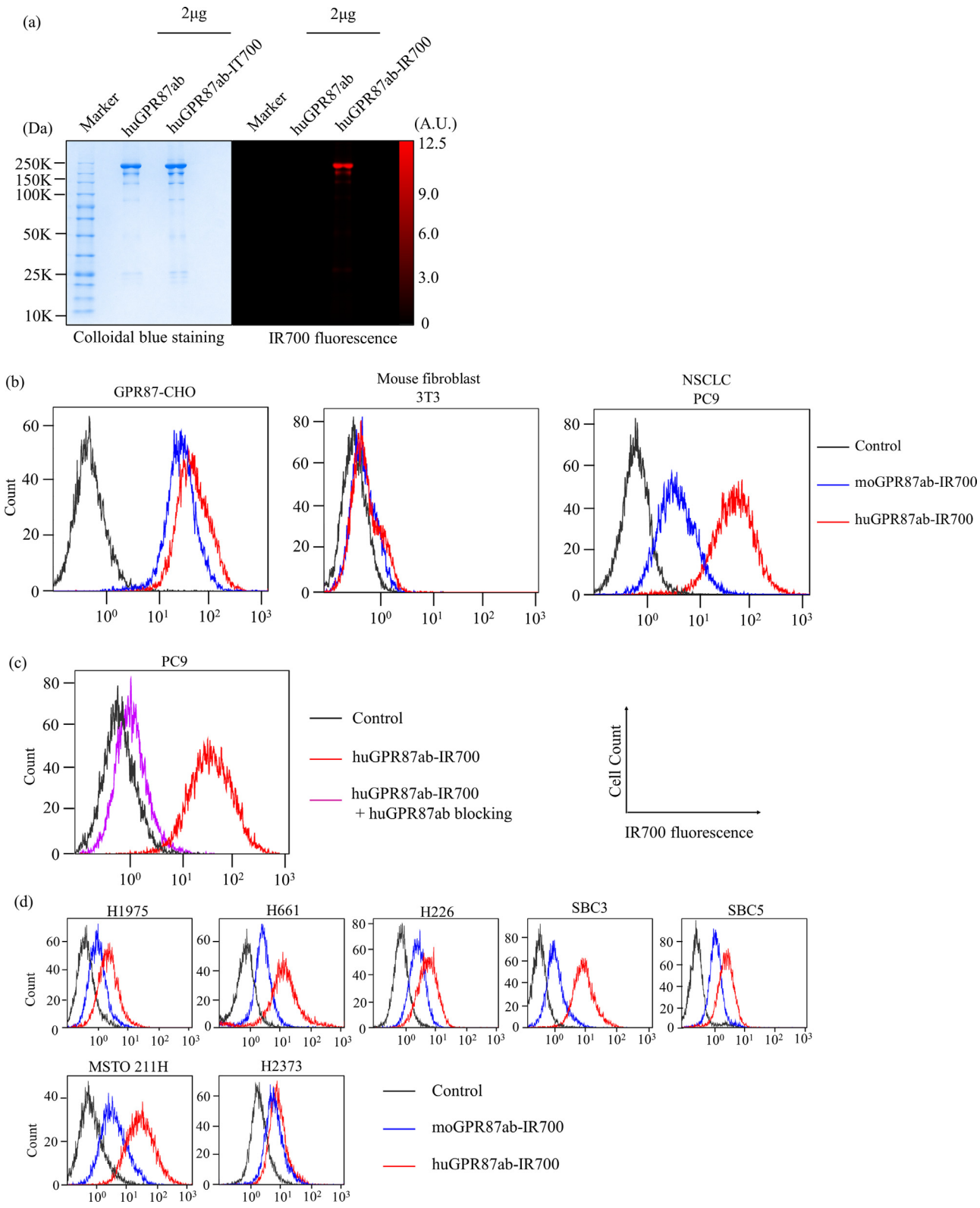

Fig. 3. Confirmation of huGPR87ab-IR700 conjugate construction and binding ability.

(**a**) Validation of huGPR87ab-IR700 by SDS-PAGE (left: colloidal blue staining, right: fluorescence at 700 nm). Diluted huGPR87ab is used as a control. (**b**) Flow cytometric analysis of huGPR87ab-IR700 in GPR87-CHO, 3T3, and PC9 cells. GPR87 expression in GPR87-CHO cells is evident, while fluorescence is essentially zero in the GPR87-negative 3T3 mouse fibroblast cells. For PC9 cells, huGPR87ab has a higher affinity than moGPR87. (**c**) Prior incubation with excess huGPR87ab blocking the binding of huGPR87ab-IR700 to PC9 cells, indicating that huGPR87ab-IR700 binds specifically to GPR87. (**d**) Examination of GPR87 expression in lung cancer and malignant mesothelioma cell lines with moGPR87ab-IR700 and huGPR87ab-IR700.

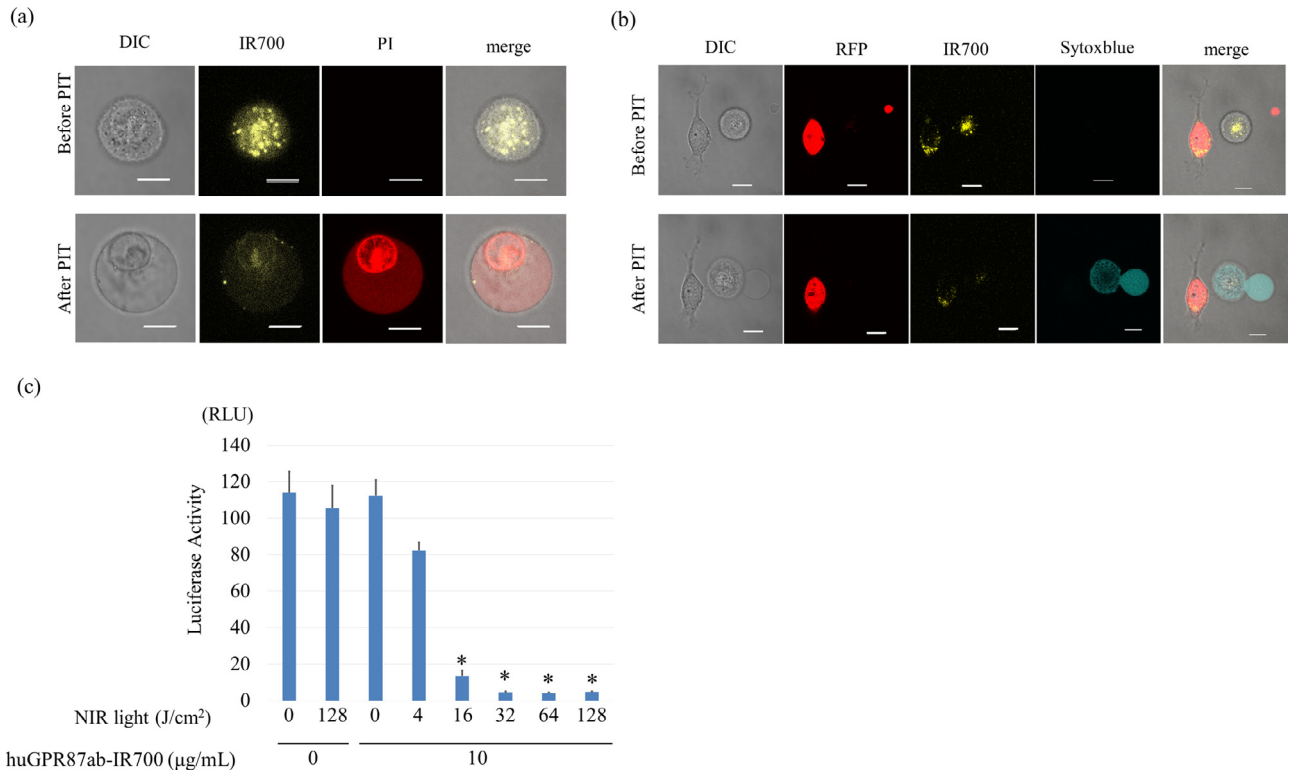

Fig. 4. *Effect of NIR-PIT with huGPR87ab-IR700 on PC9 cells in vitro.*

(**a**) NIR-PIT with huGPR87ab-IR700 on PC9 cells was observed under a microscope. The huGPR87ab-IR700 was allowed to react for 8 h or more, and images were taken before and after 64 J/cm^2 NIR irradiation. Within 30 min after NIR irradiation, the cells burst and propidium iodide (PI; necrotic cell death marker) became positive. Scale bars, 10 μm. (**b**) PC9-luc and 3T3-RFP were co-cultured and incubated with huGPR87ab-IR700, and images were taken before and after 64 J/cm^2 NIR irradiation. Only PC9 cells were ruptured by NIR irradiation and Sytox Blue (necrotic cell death marker) became positive, while 3T3-RFP remained intact. (**c**) Luciferase activity in PC9 cells treated with GPR87 targeting NIR-PIT measured in relative light units (RLUs): the activity decreased in an NIR-light dose-dependent manner. (n = 3, $^*p < 0.05$ [two-tailed unpaired t-test]). NIR, near-infrared; PIT, photoimmunotherapy.

lines. Moreover, huGPR87ab-IR700 had a higher affinity to the protein *in vitro* than moGPR87ab-IR700.

3.4. In vitro *NIR-PIT effects with huGPR87-IR700 in lung cancer and MPM cell lines*

To confirm the effect of *in vitro* GPR87-targeted NIR-PIT using optical monitoring, the PC9 cell line was genetically modified to express luciferase (PC9-luc) (Fig. S2a and b). GPR87 expression did not change after luciferase transfection (Fig. S2c).

PC9-luc cells were observed serially before and after NIR-PIT employing a fluorescence microscope. After exposure to NIR-light (64 J/cm^2), cellular swelling, bleb formation, and death were observed (Fig. 4a). No significant changes were observed in 3T3-RFP (GPR87 negative) cells (Fig. 4b). *In vitro* NIR-PIT with huGPR87-IR700 was also performed with SBC5-luc (SCLC) and H2373-luc (MPM), and similar results were obtained (Fig. S4a and b). These cellular changes were observed within 30 min after NIR-light irradiation, suggesting that necrotic cell death was rapidly induced by NIR-PIT.

Next, to quantify the effect of NIR-PIT *in vitro*, we performed a cytotoxicity assay after 24 h using luciferase activity quantitation with PC9-luc, SBC5, and H2373-luc. Luciferase activity significantly decreased in NIR-PIT-treated cells (Fig. 4c and Fig. S3c and d). In summary, NIR-PIT induced necrotic cell death and exhibited light dose-dependent manner *in vitro*.

3.5. In vivo *biodistribution of huGPR87-IR700 in tumour bearing mice*

To study the distribution of huGPR87ab-IR700 *in vivo*, we used a xenograft model in which PC9-luc cells were inoculated into the right dorsum of mice (a total of 3 mice were used in the experiment). After 200 μg of GPR87hu-IR700 injection, high fluorescence was observed across the whole mouse body; the tumour was then gradually visualised over the subsequent 1 h (Fig. 5a). The fluorescence intensity of the tumour was strongest immediately after injection and 12 h later, and the tumour-to-background ratio was highest after 12–24 h (Fig. 5b and c). No specific localisation of IR700 was observed except in the liver, kidney, and bladder, which is presumably due to hepatic and renal metabolism and urinary excretion.

In the blocking study (n = 1 per experimental group, a total 2 of mice were used in the experiment), tumour fluorescence could be clearly observed in mice injected with IgG, while not in mice blocked with GPR87 antibody. In contrast, the fluorescence in the liver and bladder was similar in both mice (Fig. S4).

These results indicated that huGPR87ab-IR700 is distributed specifically in GPR87-expressing tumours. Based on these results, we decided to administer treatment 1 day after huGPR87ab-IR700 administration.

3.6. In vivo *anti-tumour effect of NIR-PIT with huGPR87ab-IR700 in dorsal xenograft model*

To monitor the destruction of the target tumour cells induced by NIR-PIT, we examined BLI and fluorescence from mice with tumours in the right dorsum (a total of 11 mice (6 controls and 5 NIR-PIT) were used in the experiment). (Fig. 6a). Luciferase activity within the control, as determined by BLI, showed a gradual increase that was concomitant with tumour growth. In contrast, luciferase activity decreased gradually over 2 days after NIR-PIT treatment (Fig. 6b). NIR-PIT introduced on days 0 and 1 resulted in a significant decrease in the percentage of tumour volumes. (Fig. 6c). Quantitative relative light unit (RLU) was significantly reduced in NIR-PIT treated tumours (Fig. 6d). In summary, GPR87-targeted NIR-PIT with huGPR87ab-

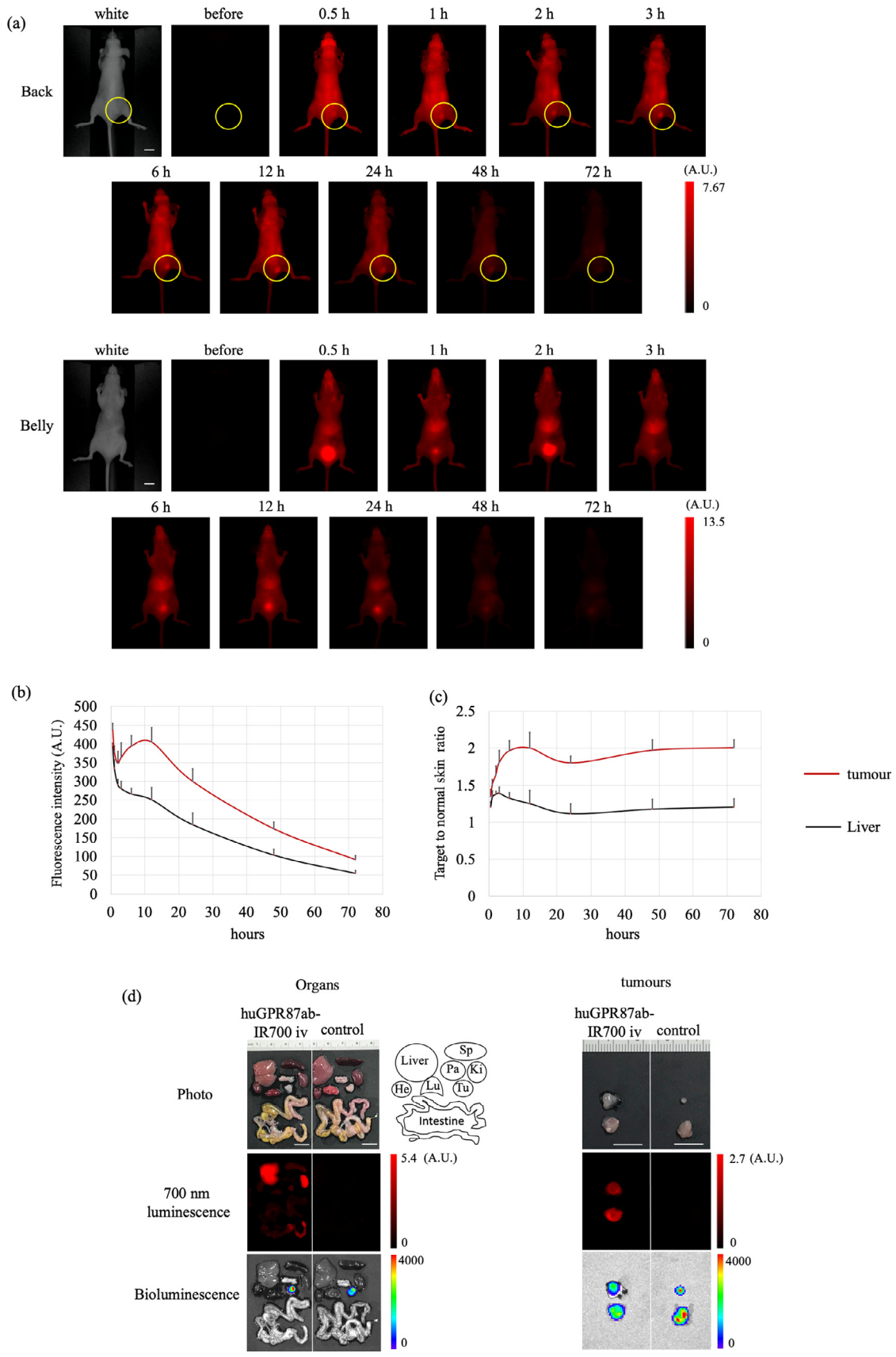

Fig. 5. In vivo biodistribution of huGPR87ab-IR700.

(**a**) Representative images before and after intravenous injection of huGPR87ab-IR700 (fluorescence imager, 700 nm). The fluorescence intensity of the signal increases up to 12 h post-injection and then gradually decreases until it became undetectable 3 days after injection. Signals in the bladder are observed 0.5 h after injection, and liver accumulation lasts for 1 day after injection. Scale bars, 1 cm. (**b**) Fluorescence intensity measurement of the tumour and liver. Signal accumulation in the tumour is observed at 12 h after the injection ($n = 3$). (**c**) The target-to-background ratios of the tumour and liver are shown. Higher accumulation is observed in the tumour than in the liver 2 to 3 days after injection ($n = 3$). Data are mean ± SEM. (**d**) *Ex vivo* photos, fluorescence, and BLI imaging at day 1 after huGPR87ab-IR700 injection. The left image shows a mouse injected with huGPR87ab-IR700, and the right shows the control. Fluorescence is observed in the liver, intestine (faeces), and kidneys in addition to the tumour (left side images). In the enlarged image of the tumour, huGPR87ab-IR700 accumulates in the tumour (right images). (Tu, tumour; He, heart; Lu, lung; Li, liver; Pa, pancreas; Sp, spleen; Ki, kidney; In, intestine; Bl, bladder.). Scale bars, 1 cm.

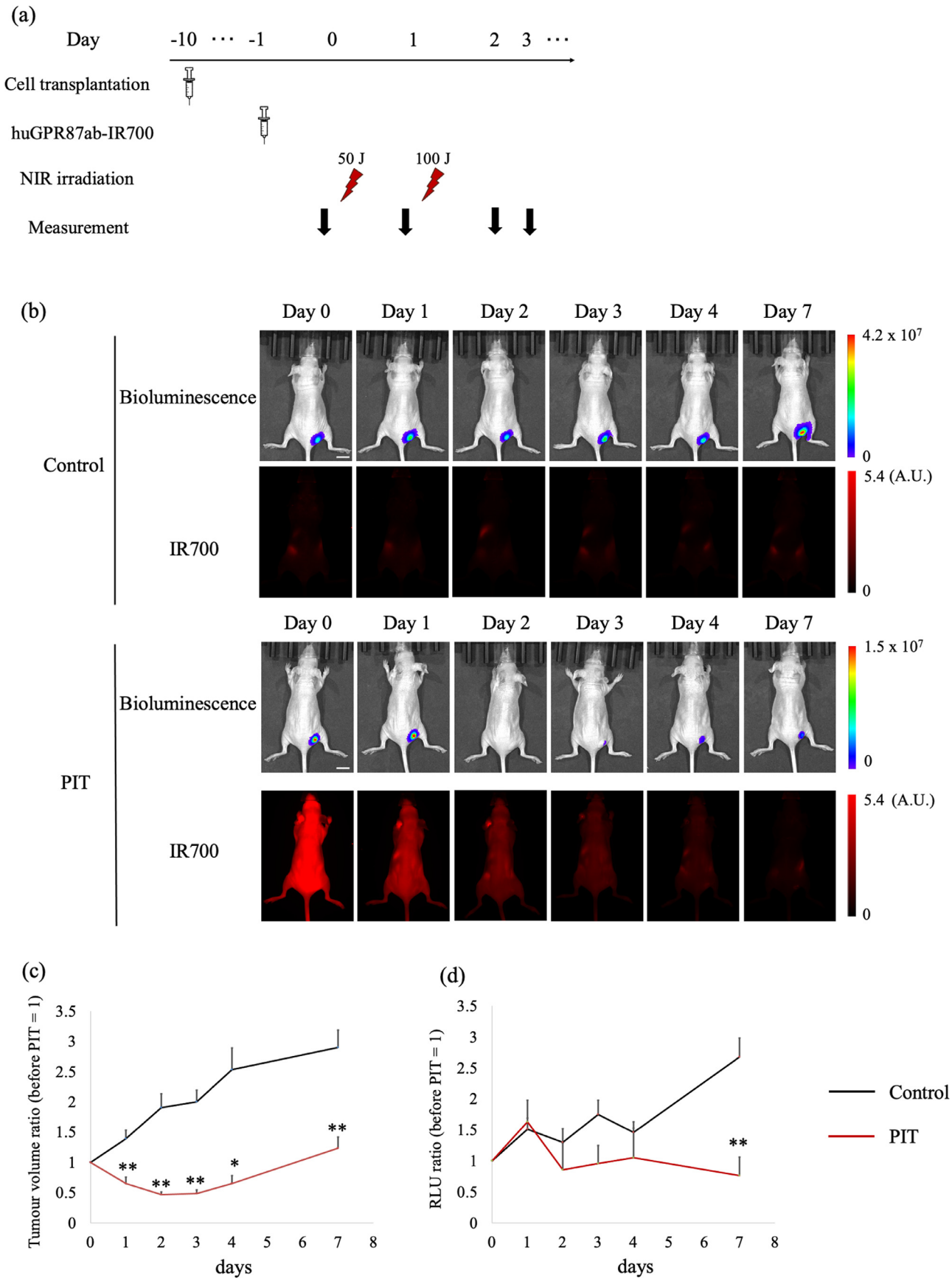

Fig. 6. In vivo GPR87 targeted NIR-PIT in mice dorsal xenograft tumour model.

(**a**) GPR87-targeted NIR-PIT regimen in a dorsal xenograft tumour model involving huGPR87ab-IR700 (200 μg) injection and NIR-light exposure (100 mW/cm^2) is shown in a line. (**b**) *In vivo* BLI and fluorescence of tumour-bearing mice. In the NIR-PIT group, luminescence decreases after NIR-light irradiation. Scale bars, 1 cm. (**c**) Tumour volume ratio is shown (before NIR-PIT = 1). NIR-PIT introduced on days 0 and 1 leads to significant reductions in the tumour volume (at day 1: $p = 0.0058$; day 2: $p = 0.0005$, day 3: $p = 0.0001$; day 4: $p = 0.0328$, at day 7: $p = 0.0029$) (control: $n = 6$, NIR-PIT: $n = 5$, $^*p < 0.05$, $^{**}p < 0.001$, [two-tailed unpaired *t*-test]). (**d**) Quantitative RLUs shows a significant decrease in GPR87-targeted NIR-PIT-treated tumours (at day 7: $p = 0.0033$) (control: $n = 6$, NIR-PIT: $n = 5$, $^{**}p < 0.001$, [two-tailed unpaired *t*-test]). NIR, near infrared; PIT, photoimmunotherapy; RLU, relative light unit.

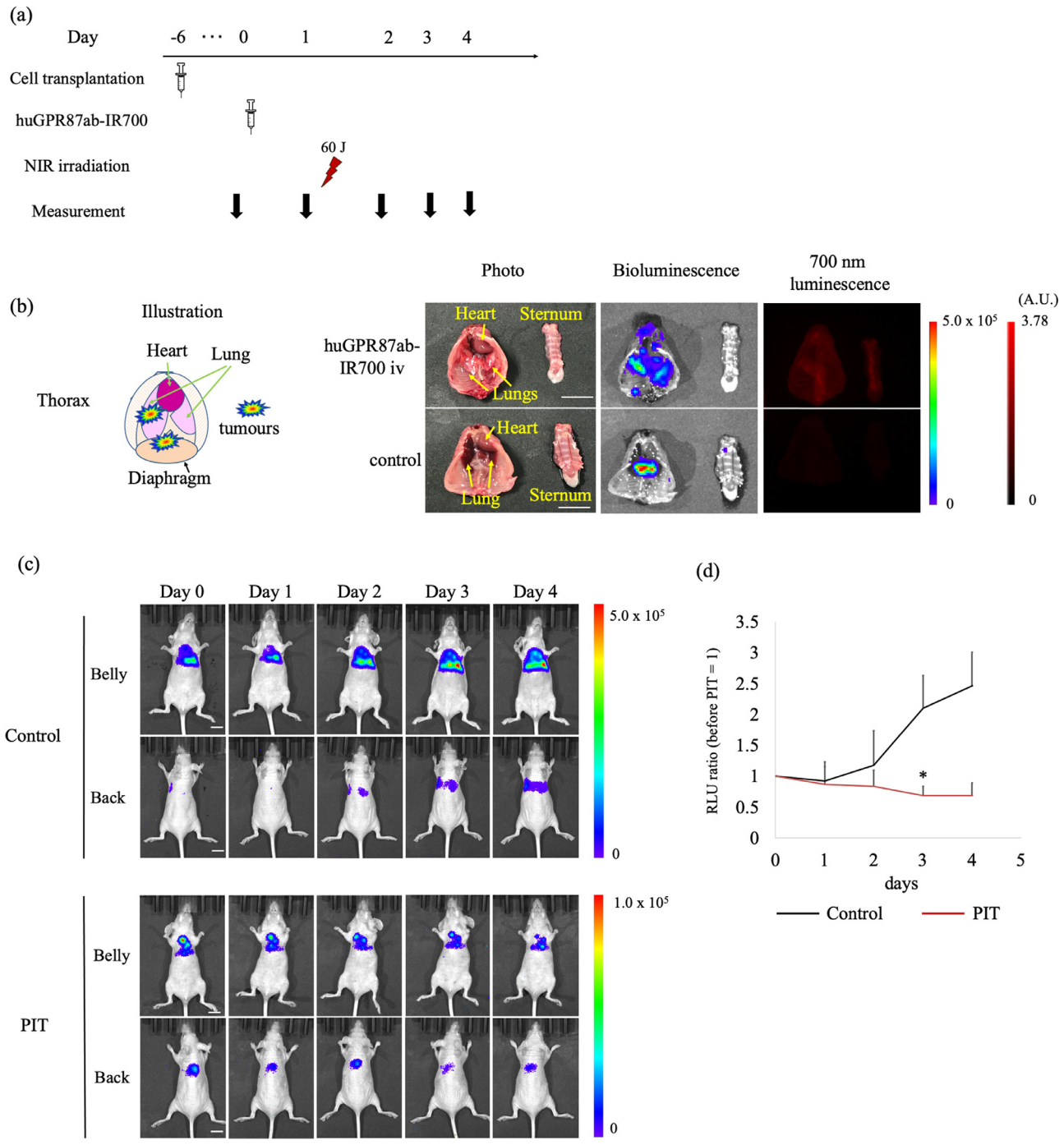

Fig. 7. In vivo GPR87 targeted NIR-PIT in a pleural disseminated xenograft model.

(**a**) GPR87-targeted NIR-PIT regimen in mice pleural disseminated tumour model involving huGPR87ab-IR700 (200 μg) injection and NIR-light exposure (60 mW/cm^2) is shown in a line. (**b**) *Ex vivo* fluorescence imaging on day 1 after huGPR87ab-IR700 injection to confirm the pleural disseminated tumour model. The tumour mass is not visible in the photograph, but pleural dissemination can be observed with bioluminescence imaging (BLI) and 700-nm fluorescence imaging throughout the thoracic cavity. Scale bars, 1 cm. (**c**) *In vivo* BLI of a mice pleural disseminated tumour model with the treatment. In the NIR-PIT group, luminescence decreases after irradiation with NIR-light. Scale bars, 1 cm. (**d**) Quantitative RLU decreases significantly in GPR87-targeted NIR-PIT-treated tumours (on day 3: $p = 0.0495$) ($n = 5$, $^*p < 0.05$, [two-tailed unpaired *t*-test]). NIR, near infrared; PIT, photoimmunotherapy; RLU, relative light unit.

IR700 was effective against the flank tumour and successfully achieved site-specific tumour ablation.

3.7. In vivo *antitumour effect of NIR-PIT in a pleural dissemination model*

To evaluate the therapeutic effect of NIR-PIT in a more clinical setting, we used a pleural dissemination model ($n = 5$ per experimental group, a total of 10 mice were used in the experiment) (Fig. 7a). We used a xenograft model in which PC9-luc cells were injected into the pleural cavity of mice fed a white diet for at least 1 week. Two hundred micrograms of the antibody were injected via the tail vein. One day after the injection, the distribution of PC9-luc cells in the thoracic cavity was evaluated by BLI, and the distribution of antibodies was confirmed with a 700-nm fluorescence *ex vivo* ($n = 1$ per experimental group, a total of 2 mice were used for *ex vivo* imaging). Successful establishment of tumour pleural dissemination was confirmed, and the antibody was widely distributed in the pleural cavity (Fig. 7b). Up

to 4 days after NIR-PIT treatment, a decrease in bioluminescence was observed, which was significantly different from that of the control (Fig. 7c and d). NIR-PIT targeting GPR87 showed an anti-tumour effect on human lung cancer cell lines *in vivo* with a newly developed humanised antibody.

4. Discussion

GPR87 has high tumour specificity and is a promising target for cancer treatment [14]. The rate of EGFR mutation, the most common mutation in lung cancer, is 10−40%, and it is rare in NSLSCC [42−44]. In this study, 50% of NSLAC and 65.5% of NSLSCC were positive for GPR87, similar to a previous report [11]. Thus, the number of patients suitable for NIR-PIT targeting GPR87 is expected to be high, although limitations owing to disease progression are expected. It is noteworthy that this is the first study to evaluate the expression of GPR87 in SCLC and MPM specimens, which was especially expressed in MPM. As described above, although many proteins can be targeted, no definitive therapeutic method has been developed thus far. In this study, it was a great achievement to show an effective therapeutic effect by targeting GPR87.

NIR-PIT is greatly affected by antibodies and the NIR irradiation method. For the successful clinical application of the mouse antibody, it is necessary to reduce its immunogenicity via chimerisation or humanisation. Clinical experience shows that the murine variable region of the chimeric mAb induces HAMA and produces humanised antibodies [45,46]. There are many methods for developing a humanised antibody. For our study, we transplanted the CDR of a mouse antibody into a human framework. A decrease in affinity might occur when using this method, and it is necessary to maintain the affinity of the antibody by retaining the Vernier zone [47]. We confirmed the affinity of the huGPR87 antibody produced in this study and confirmed that it is higher than that of moGPR87.

Most mouse tumour models are subcutaneous transplants, but it has been reported that they differ in dynamics from tumour cells in specific organs. Therefore, it is important to evaluate a mouse model that is close to the clinical setting [48−50]. Finally, we confirmed the therapeutic effect of the human lung cancer cell line PC9 in the intrapleural dissemination model.

NIR-PIT is a modality that differs in many ways from conventional photodynamic therapy (PDT), which uses light-sensitive substances and-light irradiation. For example, in PDT the light-sensitive substance is taken up by the cells in a non-specific manner and causes cytotoxicity via oxidative stress when exposed to light, whereas in NIR-PIT the antibody-IR700 acts only on the targeting cells and damages the cell membrane when exposed to NIR-light [51,16].

The mechanism of NIR-PIT has been elucidated, *i.e.*, the binding of IR700 to the antibody and subsequent activation by NIR-light results in a change of the aggregate from hydrophilic to hydrophobic. As a result, the cell membrane is damaged, fluid flows into the cell, and the cell finally ruptures [51−53]. The contents of the necrotic cells promote the maturation of immature dendritic cells and cause immunogenic cell death. As this study was carried out in immunodeficient mice, the results would be even better in humans, where the effect is expected to be due to an immune response [53,54]. Thus, the NIR-PIT cell death mechanism is a unique, potentially new modality for MPM. Moreover, MPM rarely metastasizes and is easily controlled by this GPR87 targeting NIR-PIT.

There are a few limitations to this study. First, the number of SCLC and MPM cases is limited and may not be consistent with the incidence in clinical practice. In addition, MPM was not included in this study because sarcoma is not an indication for surgery. In the present study, we evaluated MPM and SCLC for therapeutic targeting of thoracic tumours. The high expression rate of GPR87 in MPM is very interesting and may be a new therapeutic option for MPM. We believe that the expression of GPR87 needs to be investigated in a larger number of cases. Second, the images of biodistribution in mice showed some accumulation in organs other than the tumour. This indicates that NIR-PIT may cause damage to organs. However, one of the major advantages of NIR-PIT is that the treatment site can be selected by NIR-light. We treated intrathoracic tumours in a pleural dissemination model *in vivo* without fatal adverse events. We believe that the antibodies we developed are specific enough to allow NIR-PIT. However, the accumulation of the antibody in organs may cause unexpected side effects, and it is necessary to further improve the specificity of the antibody for clinical application.

In the future, GPR87 targeting NIR-PIT is expected to be performed on GPR87-high expression tumours. Cancers in the thoracic cavity or other sites were biopsied and then evaluated for GPR87 expression. Patients with high GPR87 expression are expected to be treated with GPR87ab-IR700 followed by NIR irradiation from the body surface or transendoscopically or transdrainally using a fiber light source [55,56]. In addition, the combination of NIR-PIT and immune checkpoint inhibitors will be investigated for the specific eradication of cancer cells by enhanced immunogenic cell death [51,54].

In conclusion, the present study demonstrated the frequently expressed high levels of GPR87 in lung cancer and MPM. HuGPR87ab reacted with several cancer cell lines and selectively destroyed the cells by NIR-PIT targeting GPR87 *in vitro*. Subcutaneous or pleural disseminated lung cancer mouse models were prepared, and NIR-PIT targeting GPR87 resulted in a decrease in tumour cell activity *in vivo*. Further research is needed for clinical applications.

Contributors

HY mainly conducted the experiments. YN, KT, ST, YI, MS, and CK performed the experiments. HY, YN, KT, ST, and YI analysed the data. KI, AS and KK provided anti-GPR87 antibody and its experimental data. TT analysed specimen as a pathologist. HY, KI and KS, wrote first draft of the manuscript. HY and KS had verified the underlying data. KS designed and supervised all the study. All authors have agreed on the final version of the manuscript.

Abbreviations

NIR, near-infrared; PIT, photoimmunotherapy; IR700, IRDye700DX; huGPR87ab, humanised monoclonal anti-GPR87 antibody; moGPR87ab, mouse monoclonal anti-GPR87 antibody; GPR87ab, anti-GPR87 antibody; mAb, monoclonal antibody; HAMA, human anti-mouse antibody; MPM, malignant pleural mesothelioma; VH, heavy chain variable region; LH, light chain variable region; NSLAC, non-small cell lung adenocarcinoma; NSLSCC, non-small cell lung squamous cell carcinoma; SCLC, small cell lung cancer; PI, propidium iodide; RLU, relative light unit; CDR, complementary determining region; PDT, photodynamic therapy; FR, framework region

Data sharing statement

All data generated or analysed in this study are included. Data can be made available upon request to the corresponding author.

Declaration of Competing Interest

The authors declare that they have no known competing financial interests or personal relationships that could have appeared to influence the work reported in this paper.

Acknowledgments

We would like to thank all the members of our laboratory for their comments and suggests on this research. We also thank to the nano-

plat form at Nagoya University, and core technical staffs in Nagoya University Equipment Sharing System. We appreciate the support from the Program for Developing Next-generation Researchers (Japan Science and Technology Agency), KAKEN (18K15923, 21K07217, JSPS), FOREST- Souhatsu (JST), CREST (JST).

Supplementary materials

Supplementary material associated with this article can be found, in the online version, at doi:10.1016/j.ebiom.2021.103372.

References

[1] Fidler MM, Soerjomataram I, Bray F. A global view on cancer incidence and national levels of the human development index. Int J Cancer 2016;139:2436–46. doi: 10.1002/ijc.30382.
[2] Parkin DM, Bray F, Ferlay J, Pisani P. Global cancer statistics. CA Cancer J Clin 2005;55:74–108. doi: 10.3322/canjclin.55.2.74.
[3] Furuya S, Chimed-Ochir O, Takahashi K, David A, Takala J. Global Asbestos Disaster. Int J Environ Res Public Health 2018;15:1000. doi: 10.3390/ijerph15051000.
[4] Bibby AC, Tsim S, Kanellakis N, Ball H, Talbot DC, Blyth KG, et al. Malignant pleural mesothelioma: an update on investigation, diagnosis and treatment. Eur Respir Rev 2016;25:472–86. doi: 10.1183/16000617.0063-2016.
[5] Wu M, Li X, Liu R, Yuan H, Liu W, Liu Z. Development and validation of a metastasis-related gene signature for predicting the overall survival in patients with pancreatic ductal adenocarcinoma. J Cancer 2020;11:6299–318. doi: 10.7150/jca.47629.
[6] Yan M, Li H, Zhu M, Zhao F, Zhang L, Chen T, et al. G protein-coupled receptor 87 (GPR87) promotes the growth and metastasis of CD133+ cancer stem-like cells in hepatocellular carcinoma. PLoS One 2013;8. doi: 10.1371/journal.pone.0061056.
[7] Jiang J, Yu C, Guo X, Zhang H, Tian S, Cai K, et al. G protein-coupled receptor GPR87 promotes the expansion of PDA stem cells through activating JAK2/STAT3. Mol Ther - Oncolytics 2020;17:384–93. doi: 10.1016/j.omto.2020.01.006.
[8] Okazoe H, Zhang X, Liu D, Shibuya S, Ueda N, Sugimoto M, et al. Expression and role of GPR87 in urothelial carcinoma of the bladder. Int J Mol Sci 2013;14:12367–79. doi: 10.3390/ijms140612367.
[9] Glatt S, Halbauer D, Heindl S, Wernitznig A, Kozina D, Su KC, et al. hGPR87 contributes to viability of human tumor cells. Int J Cancer 2008;122:2008–16. doi: 10.1002/ijc.23349.
[10] Gugger M, White R, Song S, Waser B, Cescato R, Rivière P, et al. GPR87 is an overexpressed G-protein coupled receptor in squamous cell carcinoma of the lung. Dis Markers 2008;24:41–50. doi: 10.1155/2008/857474.
[11] Nii K, Tokunaga Y, Liu D, Zhang X, Nakano J, Ishikawa S, et al. Overexpression of G protein-coupled receptor 87 correlates with poorer tumor differentiation and higher tumor proliferation in non-small-cell lung cancer. Mol Clin Oncol 2014;2:539–44. doi: 10.3892/mco.2014.292.
[12] Wang L, Zhou W, Zhong Y, Huo Y, Fan P, Zhan S, et al. Overexpression of G protein-coupled receptor GPR87 promotes pancreatic cancer aggressiveness and activates NF-κB signaling pathway. Mol Cancer 2017;16:61. doi: 10.1186/s12943-017-0627-6.
[13] Tabata K, Baba K, Shiraishi A, Ito M, Fujita N. The orphan GPCR GPR87 was deorphanized and shown to be a lysophosphatidic acid receptor. Biochem Biophys Res Commun 2007;363:861–6. doi: 10.1016/j.bbrc.2007.09.063.
[14] Zhang Y, Scoumanne A, Chen X. G Protein-coupled receptor 87: a promising opportunity for cancer drug discovery. Mol Cell Pharmacol 2010;2:111–6. doi: 10.4255/mcpharmacol.10.15.
[15] Kita Y, Go T, Nakashima N, Liu D, Tokunaga Y, Zhang X, et al. Inhibition of cell-surface molecular GPR87 with GPR87-suppressing adenoviral vector disturb tumor proliferation in lung cancer cells. Anticancer Res 2020;40:733–41. doi: 10.21873/anticanres.14004.
[16] Mitsunaga M, Ogawa M, Kosaka N, Rosenblum LT, Choyke PL, Kobayashi H. Cancer cell-selective *in vivo* near infrared photoimmunotherapy targeting specific membrane molecules. Nat Med 2011;17:1685–91. doi: 10.1038/nm.2554.
[17] Sato K, Watanabe R, Hanaoka H, Harada T, Nakajima T, Kim I, et al. Photoimmunotherapy: comparative effectiveness of two monoclonal antibodies targeting the epidermal growth factor receptor. Mol Oncol 2014;8:620–32. doi: 10.1016/j.molonc.2014.01.006.
[18] Cognetti DM, Johnson JM, Curry JM, Mott F, Kochuparambil ST, McDonald D, et al. Results of a phase 2a, multicenter, open-label, study of RM-1929 photoimmunotherapy (PIT) in patients with locoregional, recurrent head and neck squamous cell carcinoma (rHNSCC). J Clin Oncol 2019;37:6014. doi: 10.1200/JCO.2019.37.15_suppl.6014.
[19] Khazaeli MB, Conry RM, LoBuglio AF. Human immune respone to monoclonal antibodies. J Immunother 1994;15:42–52. doi: 10.1097/00002371-199401000-00006.
[20] Ramirez RD, Sheridan S, Girard L, Sato M, Kim Y, Pollack J, et al. Immortalization of human bronchial epithelial cells in the absence of viral oncoproteins. Cancer Res 2004;64:9027–34. doi: 10.1158/0008-5472.CAN-04-3703.
[21] Sato K, Nakajima T, Choyke PL, Kobayashi H. Selective cell elimination *in vitro* and *in vivo* from tissues and tumors using antibodies conjugated with a near infrared phthalocyanine. RSC Adv 2015;5:25105–14. doi: 10.1039/C4RA13835J.
[22] Sato K, Nagaya T, Nakamura Y, Harada T, Choyke PL, Kobayashi H. Near infrared photoimmunotherapy prevents lung cancer metastases in a murine model. Oncotarget 2015;6:19747–58. doi: 10.18632/oncotarget.3850.
[23] Sato K, Choyke PL, Hisataka K. Selective cell elimination from mixed 3D culture using a near infrared photoimmunotherapy technique. J Vis Exp 2016;2016:8–11. doi: 10.3791/53633.
[24] Yasui H, Takahashi K, Taki S, Shimizu M, Koike C, Umeda K, et al. Near infrared photo-antimicrobial targeting therapy for Candida albicans. Adv Ther 2021:2000221. doi: 10.1002/adtp.202000221.
[25] Hanaoka H, Nakajima T, Sato K, Watanabe R. Photoimmunotherapy of hepatocellular carcinoma targeting Glypican-3 combined with nanosized albumin-bound paclitaxel. Nanomedicine 2015;10:1139–47. doi: 10.2217/NNM.14.194.
[26] Sato K, Watanabe T, Wang S, Kakeno M, Matsuzawa K, Matsui T, et al. Numb controls E-cadherin endocytosis through p120 catenin with aPKC. Mol Biol Cell 2011;22:3103–19. doi: 10.1091/mbc.E11-03-0274.
[27] Sato K, Nagaya T, Nakamura Y, Harada T, Nani RR, Shaum JB, et al. Impact of C4′-O-Alkyl linker on in vivo pharmacokinetics of near-infrared cyanine/monoclonal antibody conjugates. Mol Pharm 2015;12:3303–11. doi: 10.1021/acs.molpharmaceut.5b00472.
[28] Sato K, Gorka AP, Nagaya T, Michie MS, Nakamura Y, Nani RR, et al. Effect of charge localization on the: *in vivo* optical imaging properties of near-infrared cyanine dye/monoclonal antibody conjugates. Mol Biosyst 2016;12:3046–56. doi: 10.1039/c6mb00371k.
[29] Sato K, Gorka AP, Nagaya T, Michie MS, Nani RR, Nakamura Y, et al. Role of fluorophore charge on the in vivo optical imaging properties of near-infrared cyanine dye/monoclonal antibody conjugates. Bioconjug Chem 2015;27 acs.bioconjchem.5b00492. doi: 10.1021/acs.bioconjchem.5b00492.
[30] Nishinaga Y, Sato K, Yasui H, Taki S, Takahashi K, Shimizu M, et al. Targeted phototherapy for malignant pleural mesothelioma: near-infrared photoimmunotherapy targeting podoplanin. Cells 2020;9:1019. doi: 10.3390/cells9041019.
[31] Isobe Y, Sato K, Nishinaga Y, Takahashi K, Taki S, Yasui H, et al. Near infrared photoimmunotherapy targeting DLL3 for small cell lung cancer. EBioMedicine 2020;52:102632. doi: 10.1016/j.ebiom.2020.102632.
[32] Sato K, Sato N, Xu B, Nakamura Y, Nagaya T, Choyke PL, et al. Spatially selective depletion of tumor-associated regulatory T cells with near-infrared photoimmunotherapy. Sci Transl Med 2016;8. doi: 10.1126/scitranslmed.aaf6843.
[33] Nagaya T, Nakamura Y, Sato K, Harada T, Choyke PL, Kobayashi H. Near infrared photoimmunotherapy of B-cell lymphoma. Mol Oncol 2016;10:1404–14. doi: 10.1016/j.molonc.2016.07.010.
[34] Sato K, Watanabe R, Hanaoka H, Nakajima T, Choyke PL, Kobayashi H. Comparative effectiveness of light emitting diodes (LEDs) and lasers in near infrared photoimmunotherapy. Oncotarget 2016;7:14324–35. doi: 10.18632/oncotarget.7365.
[35] Nakajima T, Sato K, Hanaoka H, Watanabe R, Harada T, Choyke PL, et al. The effects of conjugate and light dose on photo-immunotherapy induced cytotoxicity. BMC Cancer 2014;14:389. doi: 10.1186/1471-2407-14-389.
[36] Yasui H, Nishinaga Y, Taki S, Takahashi K, Isobe Y, Sato K. Near infrared photoimmunotherapy for mouse models of pleural dissemination. J Vis Exp 2021. doi: 10.3791/61593.
[37] Sato K, Nagaya T, Choyke PL, Kobayashi H. Near infrared photoimmunotherapy in the treatment of pleural disseminated NSCLC: preclinical experience. Theranostics 2015;5:698–709. doi: 10.7150/thno.11559.
[38] Watanabe R, Sato K, Hanaoka H, Harada T, Nakajima T, Kim I, et al. Minibody-indocyanine green based activatable optical imaging probes: the role of short polyethylene glycol linkers. ACS Med Chem Lett 2014;5:411–5. doi: 10.1021/ml400533y.
[39] Sato K, Choyke PL, Kobayashi H. Photoimmunotherapy of gastric cancer peritoneal carcinomatosis in a mouse model. PLoS One 2014;9:e113276. doi: 10.1371/journal.pone.0113276.
[40] Sato K, Hanaoka H, Watanabe R, Nakajima T, Choyke PL, Kobayashi H. Near infrared photoimmunotherapy in the treatment of disseminated peritoneal ovarian cancer. Mol Cancer Ther 2015;14:141–50. doi: 10.1158/1535-7163.MCT-14-0658.
[41] Ogata F, Nagaya T, Nakamura Y, Sato K, Okuyama S, Maruoka Y, et al. Near-infrared photoimmunotherapy: a comparison of light dosing schedules. Oncotarget 2017;8:35069–75. doi: 10.18632/oncotarget.17047.
[42] Paez JG, Jänne PA, Lee JC, Tracy S, Greulich H, Gabriel S, et al. EGFR mutations in lung, cancer: correlation with clinical response to gefitinib therapy. Science (80-) 2004;304:1497–500. doi: 10.1126/science.1099314.
[43] Rosell R, Moran T, Queralt C, Porta R, Cardenal F, Camps C, et al. Screening for epidermal growth factor receptor mutations in lung cancer. N Engl J Med 2009;361:958–67. doi: 10.1056/NEJMoa0904554.
[44] Leidner RS, Fu P, Clifford B, Hamdan A, Jin C, Eisenberg R, et al. Genetic abnormalities of the EGFR pathway in African American patients with non-small-cell lung cancer. J Clin Oncol 2009;27:5620–6. doi: 10.1200/JCO.2009.23.1431.
[45] Chames P, Van Regenmortel M, Weiss E, Baty D. Therapeutic antibodies: successes, limitations and hopes for the future. Br J Pharmacol 2009;157:220–33. doi: 10.1111/j.1476-5381.2009.00190.x.
[46] De Groot AS, Martin W. Reducing risk, improving outcomes: bioengineering less immunogenic protein therapeutics. Clin Immunol 2009;131:189–201. doi: 10.1016/j.clim.2009.01.009.
[47] Safdari Y, Farajnia S, Asgharzadeh M, Khalili M. Antibody humanization methods – a review and update. Biotechnol Genet Eng Rev 2013;29:175–86. doi: 10.1080/02648725.2013.801235.
[48] McLemore TL, Eggleston JC, Shoemaker RH, Abbott BJ, Bohlman ME, Liu MC, et al. Comparison of intrapulmonary, percutaneous intrathoracic, and subcutaneous

models for the propagation of human pulmonary and nonpulmonary cancer cell lines in athymic nude mice. Cancer Res 1988;48:2880–6.
[49] Manzotti C, Audisio RA, Pratesi G. Importance of orthotopic implantation for human tumors as model systems: relevance to metastasis and invasion. Clin Exp Metastasis 1993;11:5–14. doi: 10.1007/bf00880061.
[50] Sato K, Nagaya T, Mitsunaga M, Choyke PL, Kobayashi H. Near infrared photoimmunotherapy for lung metastases. Cancer Lett 2015;365:112–21. doi: 10.1016/j.canlet.2015.05.018.
[51] Kobayashi H, Griffiths GL, Choyke PL. Near-infrared photoimmunotherapy: photoactivatable antibody-drug conjugates (ADCs). Bioconjug Chem 2020;31:28–36. doi: 10.1021/acs.bioconjchem.9b00546.
[52] Sato K, Ando K, Okuyama S, Moriguchi S, Ogura T, Totoki S, et al. Photoinduced ligand release from a silicon phthalocyanine dye conjugated with monoclonal antibodies: a mechanism of cancer cell cytotoxicity after near-infrared photoimmunotherapy. ACS Cent Sci 2018;4:1559–69. doi: 10.1021/acscentsci.8b00565.
[53] Kobayashi H, Choyke PL. Near-Infrared Photoimmunotherapy of Cancer. Acc Chem Res 2019;52:2332–9. doi: 10.1021/acs.accounts.9b00273.
[54] Kobayashi H, Furusawa A, Rosenberg A, Choyke PL. Near-infrared photoimmunotherapy of cancer: a new approach that kills cancer cells and enhances anti-cancer host immunity. Int Immunol 2021;33:7–15. doi: 10.1093/intimm/dxaa037.
[55] Okuyama S, Nagaya T, Sato K, Ogata F, Maruoka Y, Choyke PL, et al. Interstitial near-infrared photoimmunotherapy: effective treatment areas and light doses needed for use with fiber optic diffusers. Oncotarget 2018;9:11159–69. doi: 10.18632/oncotarget.24329.
[56] Maruoka Y, Nagaya T, Sato K, Ogata F, Okuyama S, Choyke PL, et al. Near infrared photoimmunotherapy with combined exposure of external and interstitial light sources. Mol Pharm 2018;15:3634–41. doi: 10.1021/acs.molpharmaceut.8b00002.